# Cardiolipin defines the interactome of the major ADP/ATP carrier protein of the mitochondrial inner membrane

Steven M. Claypool,[1] Yavuz Oktay,[1] Pinmanee Boontheung,[1] Joseph A. Loo,[1,2,3] and Carla M. Koehler[1,3]

[1]Department of Chemistry and Biochemistry, [2]Department of Biological Chemistry, David Geffen School of Medicine, and [3]the Molecular Biology Institute, University of California, Los Angeles, Los Angeles, CA 90095

Defined mutations in the mitochondrial ADP/ATP carrier (AAC) are associated with certain types of progressive external ophthalmoplegia. AAC is required for oxidative phosphorylation (OXPHOS), and dysregulation of AAC has been implicated in apoptosis. Little is known about the AAC interactome, aside from a known requirement for the phospholipid cardiolipin (CL) and that it is thought to function as a homodimer. Using a newly developed dual affinity tag, we demonstrate that yeast AAC2 physically participates in several protein complexes of distinct size and composition. The respiratory supercomplex and several smaller AAC2-containing complexes, including other members of the mitochondrial carrier family, are identified here. In the absence of CL, most of the defined interactions are destabilized or undetectable. The absence of CL and/or AAC2 results in distinct yet additive alterations in respiratory supercomplex structure and respiratory function. Thus, a single lipid can significantly alter the functional interactome of an individual protein.

## Introduction

The importance of specific protein–lipid interactions for the proper functioning of an organelle is perhaps best exemplified within the inner membrane (IM) of mitochondria, the predominant subcellular location of the unique phospholipid, cardiolipin (CL). CL is a structurally unusual phospholipid with, at physiological pH, one negative charge associated with its two headgroups, and four associated fatty acyl chains (Schlame, 2008). CL is synthesized by cardiolipin synthase, Crd1p, in the context of the matrix-facing leaflets of the mitochondrial IM (Schlame and Haldar, 1993). Newly synthesized CL undergoes a remodeling process in which saturated acyl chains are replaced with more unsaturated chains, thereby establishing a high degree of acyl chain symmetry. One pathway of CL remodeling is mediated by the CL transacylase, tafazzin (Taz1p); mutations in *TAZ1* result in the X-linked disease, Barth syndrome (Xu et al., 2006; Schlame, 2008).

Correspondence to Carla M. Koehler: Koehler@chem.ucla.edu

Abbreviations used in this paper: AAC, ADP/ATP carrier; BN-PAGE, blue native polyacrylamide gel electrophoresis; CL, cardiolipin; CNAP, consecutive nondenaturing affinity purification; cyt *c*, cytochrome *c*; ETC, electron transport chain; IM, inner membrane; IP, immunoprecipitate; LC–MS/MS, liquid chromatography–tandem mass spectrometry; OXPHOS, oxidative phosphorylation; PEO, progressive external ophthalmoplegia; RCR, respiratory control ratio; Taz1p, tafazzin; wt, wild type.

The online version of this article contains supplemental material.

CL is associated with all of the major players in oxidative phosphorylation (OXPHOS), including complexes I, III, IV, and V, and the major carrier proteins for adenine nucleotides and phosphates (Schlame et al., 2000). Further, reconstitution of complex IV and the ADP/ATP carrier (AAC) activity in vitro demonstrated a strict requirement for CL (Hoffmann et al., 1994; Sedlak and Robinson, 1999). Surprisingly, yeast lacking CL (Δ*crd1*) retain the ability to respire, albeit only in optimal but not stressful (i.e., elevated temperatures) conditions (Jiang et al., 2000). As such, it was suggested that, although not absolutely necessary for OXPHOS, CL improved the efficiency of this process and broadened the range of conditions in which it could function.

Further biochemical investigation of yeast mitochondria lacking CL support the notion that CL increases the efficiency of OXPHOS (Koshkin and Greenberg, 2000). In the yeast *Saccharomyces cerevisiae*, complexes III and IV assemble in so-called respiratory supercomplexes (Cruciat et al., 2000; Schagger and Pfeiffer, 2000; Heinemeyer et al., 2007). These respiratory supercomplexes are assembled with two complex III's as a central



The Rockefeller University Press $30.00
J. Cell Biol. Vol. 182 No. 5 937–950
www.jcb.org/cgi/doi/10.1083/jcb.200801152

scaffold ($III_2$), with either one or two complex IV's attached to either side of the $III_2$ ($III_2IV$ or $III_2IV_2$, respectively). Such an organization of respiratory complexes is hypothesized to increase the efficiency of substrate channeling; indeed, the respiratory complexes in yeast behave in vivo as a functional unit (Boumans et al., 1998). Strikingly, both the stability of the respiratory supercomplexes and the in vivo cooperation between the respiratory complexes is altered in the absence of CL (Zhang et al., 2002, 2005 ; Pfeiffer et al., 2003). Thus, in the absence of CL, structural changes in the organization of complexes are observed that are directly associated with a functional consequence.

The major ADP/ATP carrier, AAC2, also displays altered assembly and reduced function in the absence of CL (Jiang et al., 2000). AACs, or ANTs in human nomenclature, mediate the 1:1 exchange of $ADP_{in}$ and $ATP_{out}$ across the IM. By doing so, ADP is transported into the mitochondrion and phosphorylated as the ATP synthase (complex V) harnesses the proton gradient generated by the electron transport chain (ETC). Mutations in the heart and skeletal muscle specific isoform of AAC, ANT1, result in certain types of autosomal dominant and recessive progressive external ophthalmoplegia (PEO; Sharer, 2005). Interestingly, four distinct amino acid point mutations identified in authentic PEO patients can be modeled in yeast AAC2 (Fontanesi et al., 2004; Palmieri et al., 2005). Thus, the high degree of sequence similarity between yeast AAC2 and human ANT1 (54% similarity) is associated with functional similarity as well. AAC may function as a homodimer (Hackenberg and Klingenberg, 1980) and has additionally been suggested to interact with proteins implicated in certain types of apoptosis, including the voltage-dependent anion channel (VDAC or porin) of the mitochondrial outer membrane (Vyssokikh and Brdiczka, 2003). Therefore, an understanding of the AAC2 interactome will provide insight into the normal physiology of AAC2 function and its putative involvement in apoptosis and certain human diseases. Further, we investigated the importance of CL in the AAC2 interactome because studies of wild-type (wt) AAC2 in the absence of CL as well as structure–function studies of defined AAC2 mutants have demonstrated a clear importance of CL for AAC2 structure and function (Hoffmann et al., 1994; Jiang et al., 2000).

## Results

### Disorganization of multiple AAC2 complexes in the absence of CL

To investigate potential AAC2 interactions, AAC complexes were analyzed by 2D blue native/SDS-PAGE (BN/SDS-PAGE; Fig. 1 A). Consistent with previous observations (Jiang et al., 2000), the pattern of AAC complexes was strikingly different in extracts derived from Δ*crd1* mitochondria than wt mitochondria. However, in contrast to the aforementioned 1D BN-PAGE analyses of AAC that suggested that AAC assembles in only two complexes, our 2D analyses identify up to six distinct AAC-containing complexes including a very large complex (the six complexes are marked with red arrows in Fig. 1 D, top panel). In contrast to a recent report that indicated that AAC assembly is altered in yeast lacking the CL transacylase, tafazzin (Brandner et al., 2005), AAC complexes seemed by-and-large normal in Δ*taz1* extracts. Of note, the AAC antiserum also recognizes porin (revealed with asterisks, Fig. 1), which migrates at a molecular mass of 29 kD below AAC. Assembly of porin into several complexes did not change appreciably when CL composition was altered. Thus, the lower porin band on the 2D gel serves as an internal standard to compare differences in the AAC assembly state. The presence of multiple AAC complexes in wt extracts and the utter disorganization of AAC complexes in the absence of CL suggest that AAC participates in multiple distinct protein complexes, many of which either require or are stabilized by CL.

To identify the AAC2 interactome, we developed a new dual affinity tag that provides two distinct advantages over existing tags, such as the TAP tag. First, it offers two distinct affinity tags in a small package of only 25 amino acids. This should allow its incorporation onto either the N or C termini, or even within a protein. Second, both affinity purifications are followed by nondenaturing elutions thereby allowing a range of downstream analyses including 2D BN/SDS-PAGE. Thus, both complex size and subunit composition can be determined. We term the tag, which consists of a protein C epitope tag separated from a $His_{10}$ tag by a 5 amino acid linker, and strategy, CNAP, for consecutive nondenaturing affinity purification (pronounced k∂ nap).

The CNAP tag was appended onto the N-terminus of yeast AAC2 (which lacks an N-terminal mitochondrial targeting signal), but still under control of the native AAC2 promoter. Upon transformation into a Δ*aac2* strain, CNAPAAC2 localized to mitochondria (Fig. 1 B) and was expressed at endogenous levels (Fig. 1 C). Furthermore, 2D BN/SDS-PAGE immunoblots indicate that the CNAPAAC2 assembled in similar complexes as untagged AAC2 and that CNAPAAC2 complexes were drastically destabilized in the absence of CL (Fig. 1 D, bottom two panels). Worth mentioning, the CNAP tag may slightly stabilize AAC2 complexes (the relative abundance of the largest complex is greater for CNAPAAC2 than AAC2 and two complexes are more readily detected for CNAPAAC2 than AAC2 in Δ*crd1* extracts). Critically, as AAC2 is required for respiration, CNAPAAC2 completely rescued the ability of Δ*aac2* yeast to grow on respiratory media such as glycerol–ethanol (Fig. 1 E). Thus, AAC2 expression, localization, assembly, and function are not significantly altered by the CNAP tag.

### The stable association of AAC2 with respiratory supercomplexes requires CL

To define the AAC2 interactome and the impact of CL on the AAC2 interactome, a preparative scale CNAP was performed (outline of protocol depicted in Fig. 2). Compared with the negative control (Fig. 2 A, 1, Δ*aac2*[AAC2]) numerous unique bands co-affinity purified with CNAPAAC2 (2, Δ*aac2*[CNAPAAC2]). Many bands were either not detected or present at significantly reduced levels in the absence of CL (3, Δ*aac2*Δ*crd1*[CNAPAAC2]). Surprisingly, many of these bands were identified by liquid chromatography–tandem mass spectrometry (LC–MS/MS) as subunits of respiratory complex III (Fig. 2 B, red labels), respiratory complex IV (blue labels), or other mitochondrial carrier proteins (purple labels; Table S1 provides LC–MS/MS details, and is available at http://www.jcb.org/cgi/content/full/jcb.200801152/DC1).

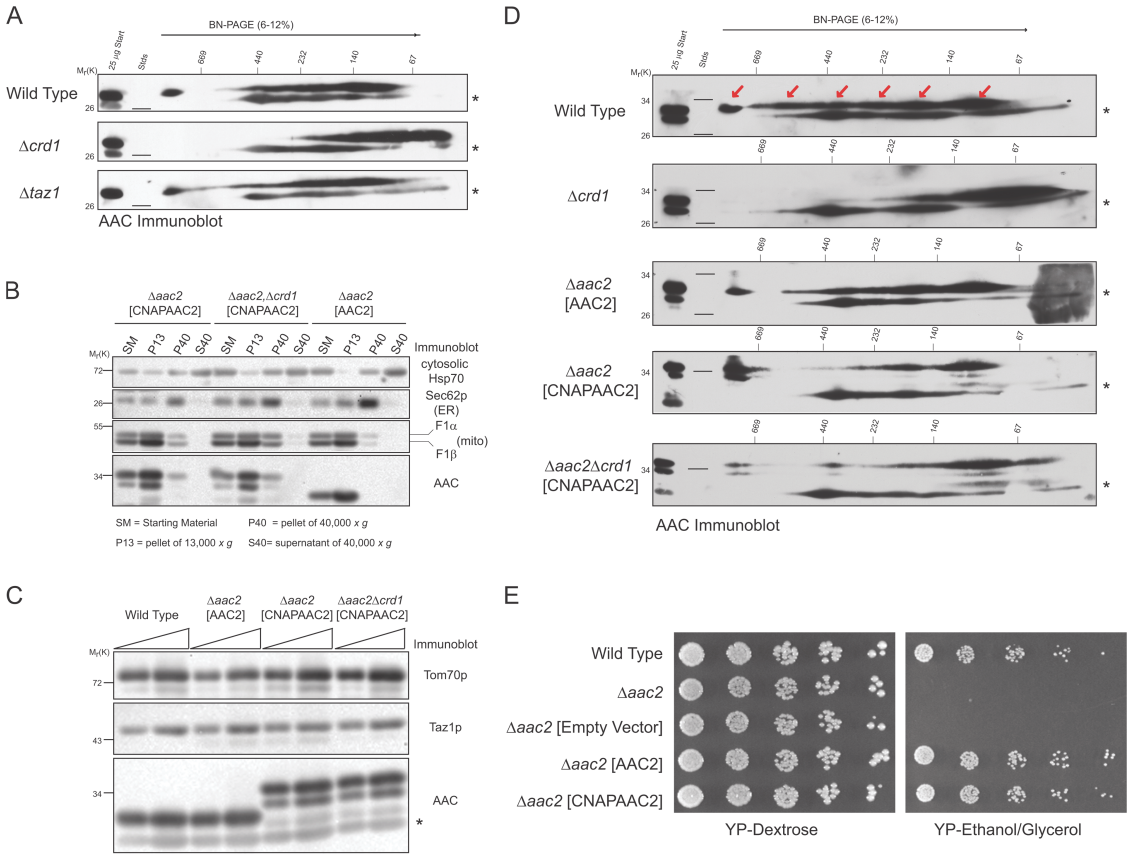


Figure 1. **Disorganization of AAC complexes in the absence of CL.** (A) 100 µg of 1.5% (wt/vol) digitonin extracts from mitochondria derived from the indicated strains were resolved by 2D BN/SDS-PAGE and AAC-complexes revealed by immunoblot. *n* = 3. (B) 25 µg of each subcellular fraction was immunoblotted for the indicated subcellular organelle. *n* = 2. (C) Steady-state expression was determined from whole cell extracts (5 and 10 µl) by immunoblotting for AAC (bottom), with Taz1p (middle) and Tom70p (top) serving as loading controls. *n* = 3. (D) CNAPAAC2 assembles in similar complexes as untagged AAC2. *n* = 3 (E) Serial dilutions of the strains indicated at the left were spotted onto YP medium with dextrose or ethanol–glycerol as the carbon source and incubated at 30°C for 3 d. *n* = 3. Asterisk highlights cross-reaction with porin of the AAC antiserum.

To confirm a subset of these interactions, CNAP was performed with the AAC2 panel and the final concentrated eluates analyzed by immunoblot for various mitochondrial proteins (Fig. 2 C). Indeed, CNAPAAC2 co-affinity purified respiratory complexes III (Cor1p, Cor2p, and Cyt1p) and IV (Cox2p and Cox4p), but not respiratory complex V (F1α or F1β), Mia40p, Yta10p, or Tim22p (see Fig. S1, available at http://www.jcb.org/cgi/content/full/jcb.200801152/DC1), all resident to the mitochondrial IM, or the outer membrane proteins porin or Tom70p. Critically, none of these proteins, including AAC2, was detected when CNAP was performed using extracts containing either untagged AAC2 or the CNAP tag appended to an unrelated mitochondrial IM protein (Fig. 2 C and Fig. S1). Interestingly, the abundance of complex III and IV subunits that co-affinity purified with CNAPAAC2 was drastically reduced in the absence of CL.

Unfortunately, we do not currently have antibodies against the numerous carrier proteins identified as interacting with AAC2. Therefore, we turned to a genetic approach to independently validate these interactions (Fig. 2 D). Specifically, we tested whether deletion of AAC2 was synthetic lethal with deletion of the phosphate carrier (Pic1p product of *MIR1*) and the GTP/GDP transporter (Ggc1p), with the reasoning that their physical association might be important for mitochondrial function under suboptimal conditions, as has been shown in the TIM22 pathway (Koehler et al., 2000). Indeed, in contrast to Δ*aac2*, Δ*mir1*, and Δ*ggc1* single deletion strains, Δ*aac2*Δ*mir1* and Δ*aac2*Δ*ggc1* double deletion strains exhibited synthetic lethal interactions based on their inability to grow on dextrose media at 37°C. These genetic interactions suggest that the newly defined physical associations between AAC2 and Pic1p and Ggc1p are important for their function in the IM.

The identification of 6 of the 10 complex III subunits (COB, Qcr6p, Qcr8p, and Qcr9p were not identified) and 6 of the 11 complex IV subunits (Cox1p, Cox3p, Cox7p, Cox8p, and Cox9p were not identified) implied that AAC2 interacts with either intact individual respiratory complexes III and/or IV, or perhaps with the respiratory supercomplexes. To determine if it is the latter, the concentrated eluates were analyzed by 2D BN/SDS-PAGE after preparative CNAP. In comparison to the negative control untagged AAC2 (Fig. 3 A), many proteins were detected in samples generated from extracts containing CNAPAAC2 (Fig. 3, B and C). Whereas many bands co-migrated in similarly sized AAC2-containing complexes, especially evident for the largest AAC2-containing complexes, there were unique bands that migrated in different-sized complexes, consistent with the notion that AAC2 participates in several distinct protein complexes.

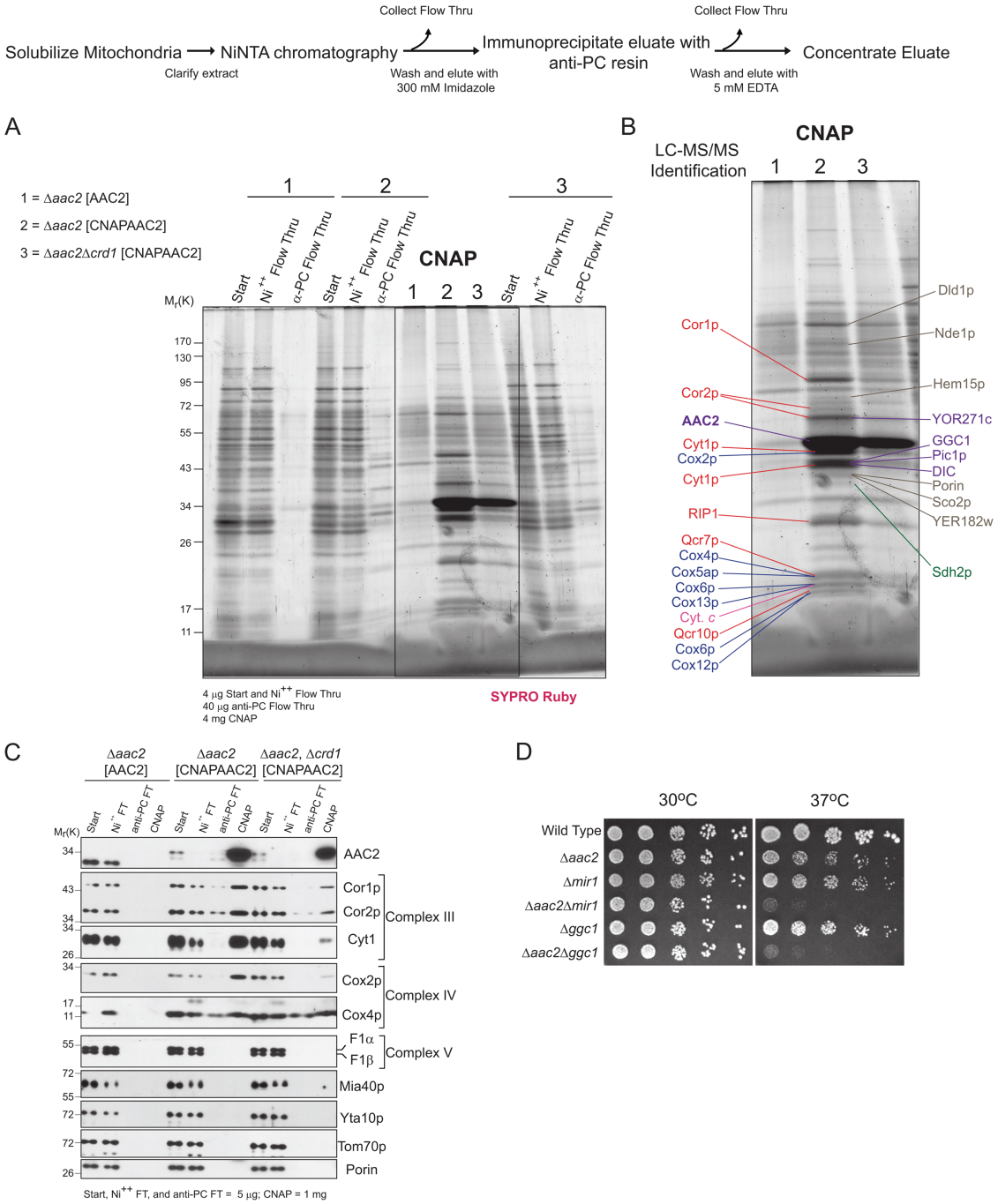


Figure 2. **1D analysis of the AAC2 interactome with and without CL.** (A) After CNAP of extracts derived from the indicated mitochondria, the final concentrated eluates were resolved by 10–15% SDS-PAGE. (B) SYPRO Ruby detected bands were extracted, digested with trypsin, and proteins identified by LC–MS/MS. Respiratory complex III and IV subunits are labeled in red and blue, respectively, and members of the mitochondrial carrier family in purple. (C) After CNAP, the final concentrated eluates were resolved by SDS-PAGE and immunoblotted for the indicated mitochondrial proteins. $n = 3$. (D) Serial dilutions of the strains indicated at the left were spotted onto YP medium with dextrose as the carbon source and incubated at the indicated temperature for 3 d.

Furthermore, as demonstrated when CNAPAAC2 was purified in the absence of CL (Fig. 3 C), some of these complexes either absolutely require CL or instead are stabilized by CL. Specifically, the cohort of bands in the largest AAC2-containing complex migrated in a smaller-sized complex, and a new collection of bands copurified in the 440-kD range. Upon protein assignment by LC–MS/MS, AAC2 did in fact co-affinity purify respiratory supercomplexes; additionally, several mitochondrial carriers were identified in AAC2 complexes that range in size from ~400–160 kD (Table S2 provides LC–MS/MS details for Fig. 3 B, and is available at http://www.jcb.org/cgi/content/full/jcb.200801152/DC1). In the presence of CL, many of the analyzed bands provided identifications for both complex III and complex IV subunits. In contrast, when CL was absent, only

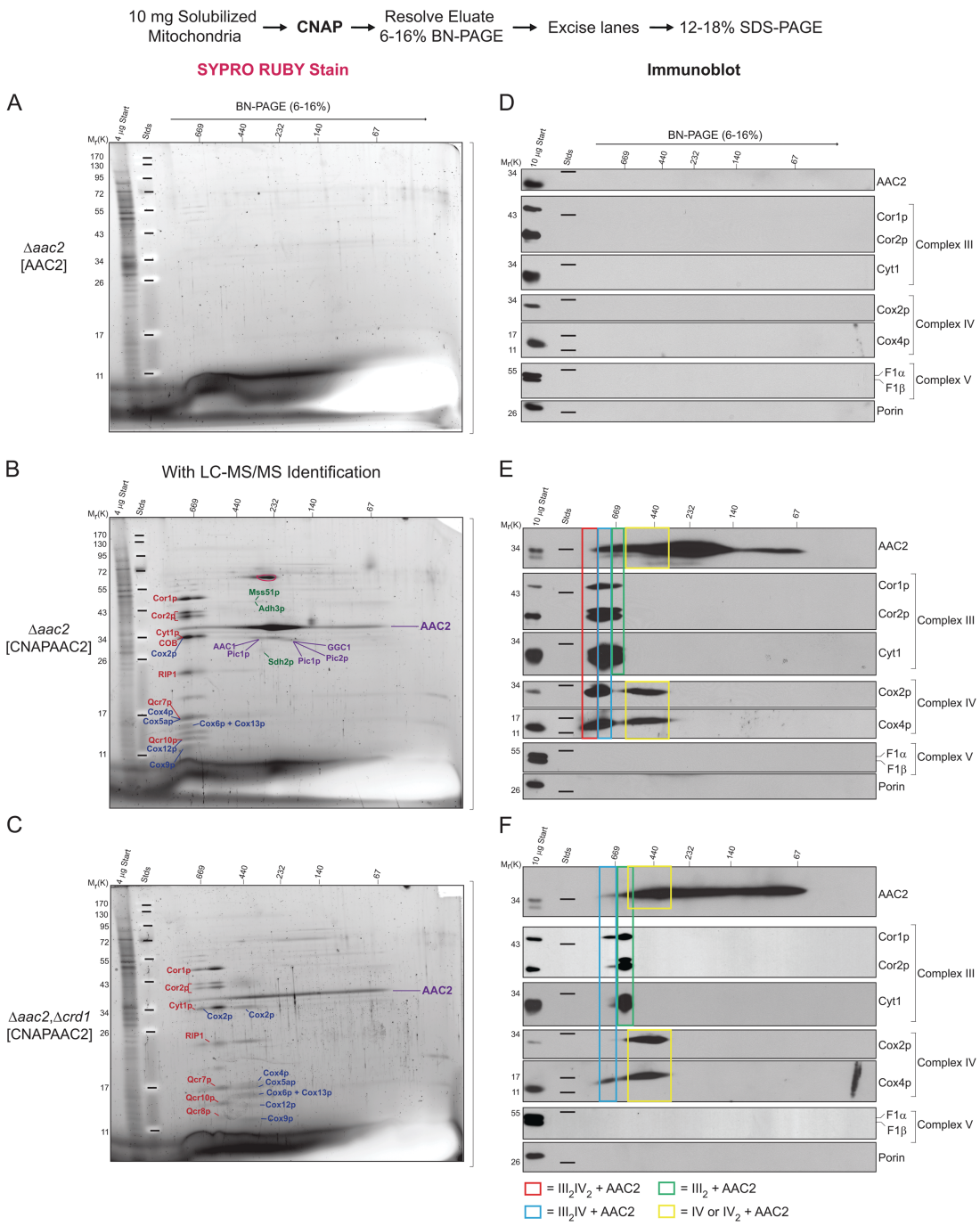


Figure 3. **2D BN/SDS-PAGE analysis of the AAC2 interactome with and without CL.** (A–C) After CNAP, the final concentrated eluates were resolved in the first dimension by 6–16% BN-PAGE and in the second dimension by 12–18% SDS-PAGE. SYPRO Ruby detected bands were extracted, digested with trypsin, and proteins identified by LC–MS/MS. Respiratory complex III and IV subunits are labeled in red and blue, respectively, and members of the mitochondrial carrier family in purple. The pink circle highlights contaminating catalase (verified by LC–MS/MS) from the BN-PAGE molecular weight markers. (D–F) After CNAP, the final concentrated eluates were resolved by 2D BN/SDS-PAGE and immunoblotted for the indicated mitochondrial proteins. $n = 3$. The sources of the purified extracts were (A and D) Δ*aac2*[AAC2], (B and E) Δ*aac2*[CNAPAAC2], and (C and F) Δ*aac2*Δ*crd1*[CNAPAAC2].

one band gave a weak dual hit for subunits of both complex III and IV (Cyt1p and Cox2p; Table S3 provides LC–MS/MS details for Fig. 3 C, and is available at http://www.jcb.org/cgi/content/full/jcb.200801152/DC1). Instead, in the absence of CL, the largest complex contained respiratory complex III subunits and the novel complex of ~440 kD represented AAC2-associated respiratory complex IV.

Immunoblots performed on purified samples derived from extracts containing untagged AAC2 and resolved by 2D BN/SDS-PAGE were entirely blank (Fig. 3 D, top series of panels). In contrast, a range of AAC2 complexes were identified after 2D BN/SDS-PAGE analyses of purified samples derived from extracts containing CNAPAAC2 and CL; the largest complex includes co-purified respiratory supercomplexes (Fig. 3 E,

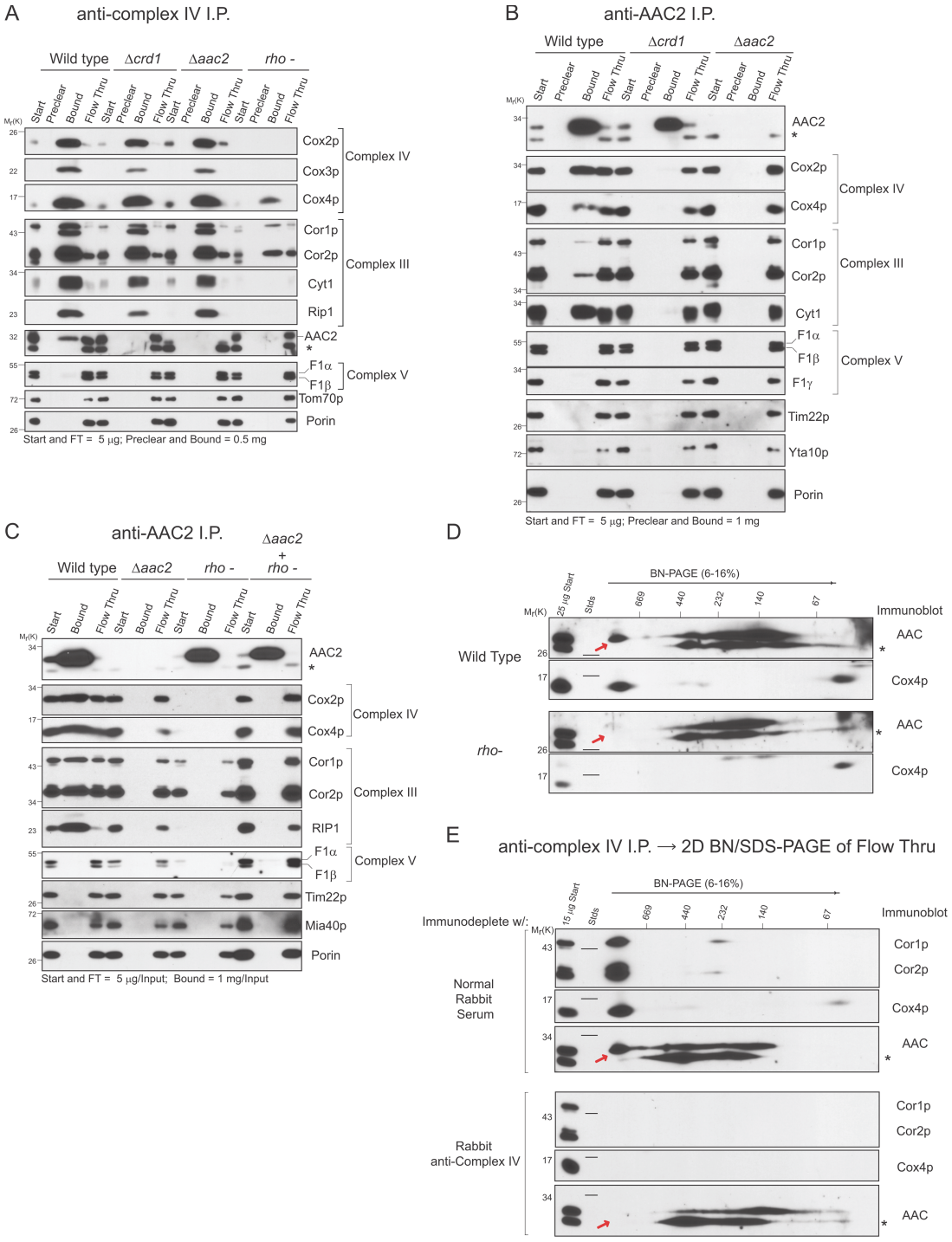


Figure 4. **The largest AAC2-containing complex requires the presence of respiratory supercomplexes and is stabilized by CL.** (A) Endogenous AAC2 coIPs with the respiratory supercomplex. An anti-complex IV IP was performed on digitonin extracts from the indicated mitochondria. 1% of the starting material and final flow-thru versus 100% of the preclear and IP beads post-washing were immunoblotted for the indicated mitochondrial proteins. *n* = 3. (B) Endogenous respiratory subunits coIP with AAC2. As in (A), except that 0.5% of the starting material and final flow-thru were analyzed. *n* = 3. (C) AAC2 and respiratory supercomplexes interact in organello. The anti-AAC2 IP was as in (B), except the preclear was omitted and the amount of protein analyzed is expressed as per mitochondrial source. *n* = 3. (D) wt or *rho*– mitochondrial extracts were resolved by 2D BN/SDS-PAGE and immunoblotted for the indicated mitochondrial proteins. *n* = 3. (E) After IP of wt digitonin extracts with normal rabbit serum or the anti-complex IV antiserum, the concentrated nonbinding flow-thrus were resolved by 2D BN/SDS-PAGE and immunoblotted for the indicated mitochondrial proteins. *n* = 3.

middle series of panels). In the absence of CL, the abundance of detected co-affinity purifying complex III and IV subunits, the size of the detected complexes, and the overlap between complex III- and IV-containing complexes were all diminished (Fig. 3 F, bottom series of panels). Based on the reported sizes of the respiratory supercomplexes (1,000 and 850 kD for $III_2IV_2$ and $III_2IV$, respectively) and the co-migration, or not, of complex III and IV subunits, we conclude that AAC2 does in fact physically

associate with respiratory supercomplexes (red boxes highlight AAC2 + $III_2IV_2$ and blue boxes AAC2 + $III_2IV$). Whether the readily detected complex $III_2$ only (green boxes) or complex IV only (yellow boxes) AAC2-containing complexes reflect true associations between AAC2 and the individual respiratory complexes or instead is caused by some degree of destabilization of respiratory supercomplexes during BN-PAGE is unclear.

Next, we determined if endogenous AAC2 and respiratory supercomplexes interact by performing reciprocal coimmunoprecipitation (coIP) analyses using a rabbit antiserum raised against intact complex IV and a monoclonal antibody specific to the N terminus of AAC2 (Panneels et al., 2003) (Fig. 4, A and B). We rationalized that if an antiserum specific for complex IV coIPed complex III, than it is in fact IPing intact respiratory supercomplexes. Indeed, after IP of complex IV from wt mitochondrial extracts, both complex IV and III subunits, but not complex V, Tom70p, or porin, were detected by immunoblot (Fig. 4 A). Importantly, endogenous AAC2 coIPed with the respiratory supercomplex. In contrast, while complex III still coIPed with complex IV in the absence of either AAC2 or CL, no AAC2 was detected. As an additional control, mitochondria derived from yeast lacking mitochondrial DNA (*rho*–) were analyzed. Several subunits of both respiratory complexes III and IV are encoded by the mitochondrial genome; as such, in *rho*– yeast, respiratory supercomplexes are not formed (Fig. 4 D). Significantly, even though AAC2 is expressed at wt levels in either the absence of CL or the mitochondrial genome, AAC2 was not detected after an anti-complex IV IP. Moreover, after IP of AAC2 from wt extracts, both complex III and IV subunits, but not complex V, Tim22p, Yta10p, or porin, were detected by immunoblot (Fig. 4 B). No proteins were detected by immunoblot when AAC2 was IPed from extracts lacking either AAC2 or CL. To address the possibility that the detected interactions occurred post-solubilization as opposed to in organello, we performed a mixing experiment with Δ*aac2* (source of respiratory supercomplexes) and *rho*– (source of AAC2) mitochondria (Fig. 4 C). After solubilization, Δ*aac2* and *rho*– extracts were combined, AAC2 IPed, and coIPed proteins detected by immunoblot. In contrast to wt extracts (all proteins expressed in same membranes), complex III and IV subunits failed to coIP with AAC2 when these proteins were expressed in separate membranes (Fig. 4 C, Δ*aac2* + *rho*–) even though AAC2 was readily IPed. Thus, the interaction of AAC2 and the respiratory supercomplex occurred within mitochondria and not nonspecifically after lysis.

Finally, we sought to confirm that the largest AAC2 complex observed in wt extracts (i.e., endogenous AAC2) is in fact AAC2 physically associated with the respiratory supercomplex by two independent means. First, in *rho*– extracts, the largest AAC2 complex was not detected (Fig. 4 D, red arrows). In contrast to Δ*crd1* extracts, only the largest AAC2 complex is affected by the absence of mitochondrial DNA. Second, the nonbinding flow-thru after IP of wt extracts with either control antiserum (normal rabbit serum) or the anti-complex IV antiserum was analyzed by 2D BN/SDS-PAGE and immunoblotting (Fig. 4 E). As expected, normal rabbit serum failed to immunodeplete any respiratory complexes and respiratory supercomplexes and all of the AAC2-complexes were detected in the flow-thru. In contrast, quantitative IP of complex IV resulted in the complete immunodepletion of respiratory supercomplexes and the selective immunodepletion of the largest AAC2 complex. Thus, endogenous AAC2 (~0.5–1% of the total AAC2 content) physically associates with the respiratory supercomplex and this interaction either requires or at the very least is stabilized by CL.

### AAC2 and CL are required for the normal structure and function of respiratory supercomplexes

Next, we sought to determine if the structure and/or function of the respiratory supercomplexes was altered in the absence of either AAC2 or CL individually or in combination, or, as suggested (Brandner et al., 2005), in the absence of the CL transacylase, tafazzin (Δ*taz1*). Our rationale for focusing on the function of the respiratory chain is that, depending on the substrate used, it measures either the function of individual complexes or the cooperative functioning of multiple complexes. Given that the association of AAC2 with the respiratory supercomplexes is uniting two individual multi-protein complexes and three unique functions, using the battery of assays available to probe OXPHOS to us, offers the best method to begin dissecting the functional relevance of the unexpected interaction of AAC2 and the respiratory supercomplexes. Because AAC2 is required for respiratory growth, the mitochondria used in all of the remaining studies were harvested from strains grown with dextrose as the sole carbon source. No major differences in the steady-state expression of various mitochondrial proteins was observed between the strains (Fig. 5 A), except for Cox2p and Cox4p, which were reduced by ~50% in Δ*crd1* backgrounds, consistent with previous observations (Zhang et al., 2003). Thus, any alteration in the assembly and/or function of the respiratory supercomplexes in the absence of AAC2, CL, both, or Taz1p, is not due to drastic effects on the stability of subunits of respiratory complexes III and/or IV.

Next, we measured the phospholipid profile of each strain's mitochondria (Fig. 5 B). In the Δ*crd1* mitochondria, CL was undetectable and phosphatidylglycerol (PG), the precursor phospholipid in CL biosynthesis, accumulated. The phospholipid profile of the Δ*aac2*Δ*crd1* mitochondria was indistinguishable from Δ*crd1* mitochondria, demonstrating that with respect to the phospholipid profile, the absence of Crd1p is dominant over that of AAC2. As expected, in the absence of Taz1p, the abundance of CL was reduced and the intermediate in the CL-remodeling pathway, monolyso-CL, amassed. The phospholipid profile of the Δ*aac2* mitochondria was statistically identical to wt mitochondria. Therefore, any alterations in the structure and/or function of the respiratory supercomplexes when AAC2 is missing are not caused by alterations in the phospholipid profile.

The respiratory supercomplexes were analyzed by BN-PAGE and 2D BN/SDS-PAGE performed in parallel followed by immunoblotting for complex III (Cyt1p and Cor2p), complex IV (Cox2p), and complex V (F1β; Fig. 5 C). In wt extracts, the relative abundance of the $III_2IV_2$ supercomplex was greater than the $III_2IV$ supercomplex, some free $III_2$ was observed, and all complex IV assembled with $III_2$ (either as $III_2IV_2$ or $III_2IV$). The profile observed for the Δ*taz1* extracts was

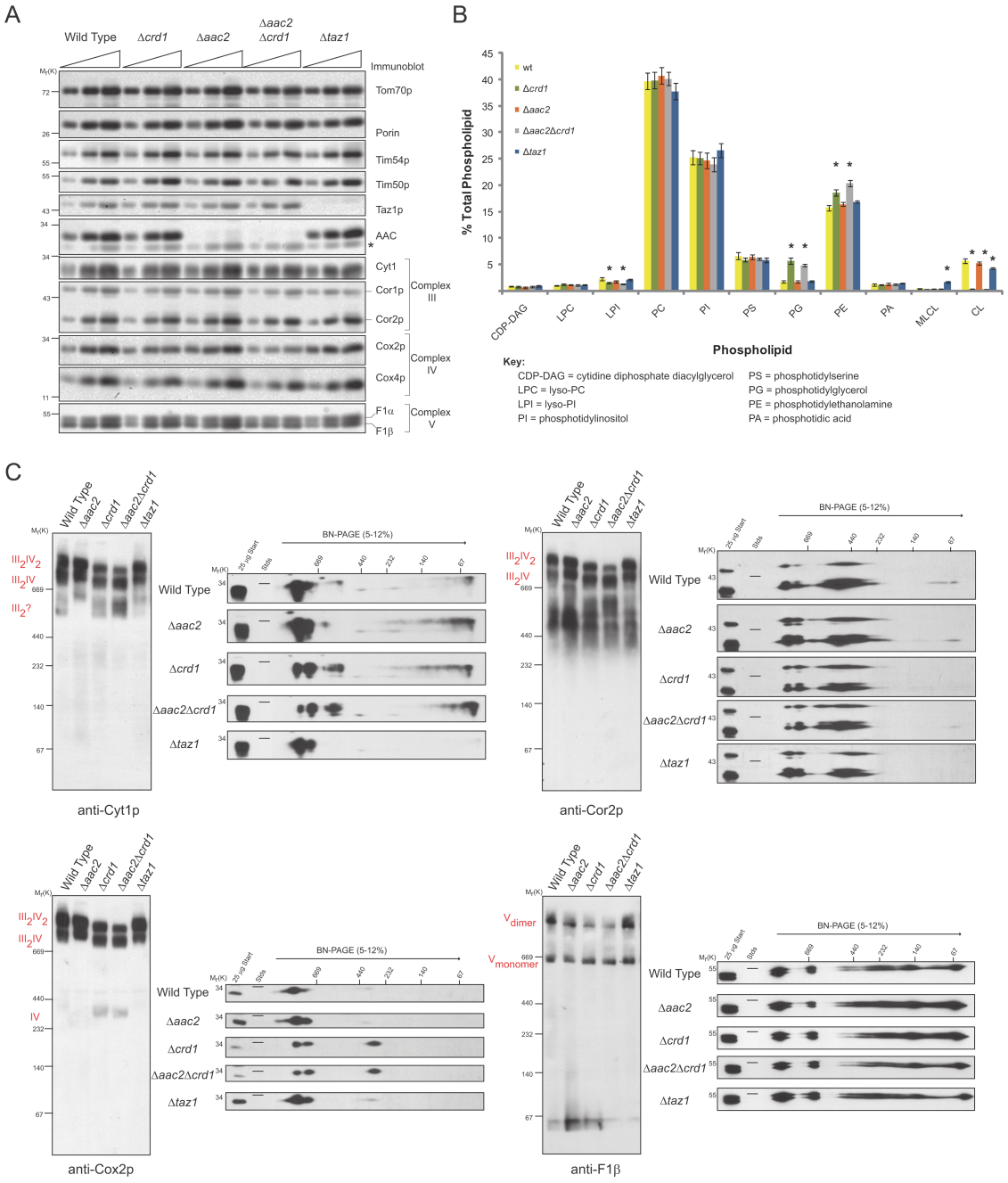


Figure 5. **AAC2 and CL are required for the normal configuration of the respiratory supercomplexes.** (A) Steady-state expression of assorted proteins (5, 10, and 20 µg protein) in the indicated mitochondria as assessed by immunoblot. $n = 3$. (B) After steady-state labeling with $^{32}P_i$, phospholipids were extracted from the indicated strains, separated by TLC, and revealed by phosphorimaging. The relative abundance of each phospholipid is expressed as a percentage of the total phospholipid in each strain (mean ± SEM, $n = 3$). Asterisks indicate significant accumulation of the designated phospholipid for a given mutant strain relative to wt ($P \leq 0.013$) as determined by one-way anova, with Holm–Sidak pairwise comparisons. (C) Mitochondrial extracts from the indicated strains were resolved by both 1D BN-PAGE and 2D BN/SDS-PAGE, performed in parallel, and immunoblots performed for complex III (Cyt1 and Cor2p), complex IV (Cox2p), and complex V (F1β). The migrations of the $III_2IV_2$, $III_2IV$, $III_2$, IV, $V_{dimer}$, and $V_{monomer}$ supercomplexes are indicated, where appropriate, in the 1D BN-PAGE immunoblots. $n = 4$.

identical to wt extracts, in contrast to a previous paper (Brandner et al., 2005). Worth noting, the Δ*taz1* strain used by Brandner et al. (2005) contained the *his3Δ200* allele, which is known to confound phenotypic analyses in yeast lacking CL (Zhang et al., 2003); as such, we speculate that the discrepant results reported here and in a previous paper are due to strain differences. In the absence of AAC2, there were subtle but consistent alterations observed in the arrangement of the respiratory supercomplexes. First, the amount of the $III_2IV$ supercomplex relative to the $III_2IV_2$ was greater than wt (most obvious in the 2D analyses). Second, the $III_2IV$ supercomplex migrated as a larger more defined entity in the absence of AAC2. Third, what is assumed to represent $III_2$ migrated as a larger more defined complex than in wt extracts. However, as in wt extracts, all complex IV

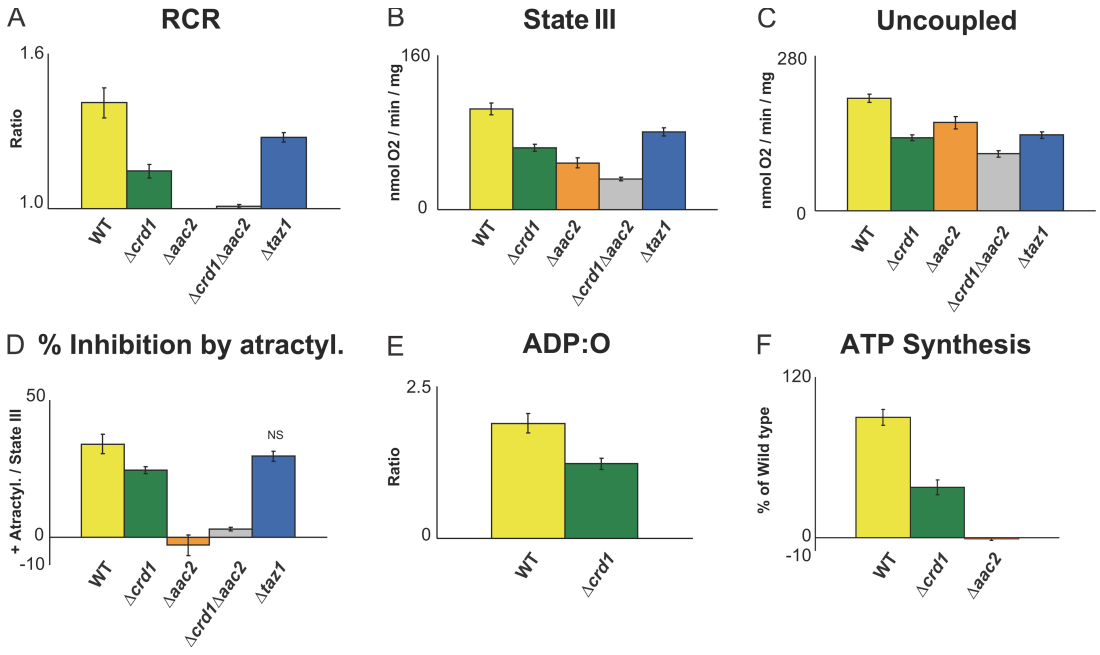


Figure 6. **AAC2 and CL are required for the optimal functioning of the respiratory supercomplexes.** 200 µg mitochondria were incubated in respiration buffer at 25°C and oxygen consumption was monitored in the presence of 5 mM succinate. (A) RCRs, (B) state III respiratory rates in the presence of 50 µM ADP, (C) uncoupled respiratory rates in the presence of 10 µM CCCP, (D) percent inhibition by 40 µM atractyloside compared with state III rates (mean ± SEM). (E) ADP:O ratios in the presence of 2 mM NADH, (F) ATP production (percentage of wt) by complex V in the presence of 5 mM NADH, 2 mM ADP, and 10 µM adenylate kinase inhibitor, $Ap_5A$ (mean ± SEM). Aliquots taken at 30, 60, 90, 120, and 150 s after addition of 2 mM ADP were extracted with PCA and ATP levels measured. Unless indicated by "NS", all differences compared with wt are statistically significant ($P \leq 0.05$) by *t* test. $n = 6–11$ (A–D), $n = 5–9$ (E), and $n = 4$ (F).

was associated with complex III (i.e., lack of free complex IV). Consistent with previous studies, all supercomplexes migrated faster in the absence of CL and the relative abundance of the $III_2IV$ to $III_2IV_2$ supercomplex was increased; this change in ratio of supercomplexes reflects a selective destabilization in complex IV association, as indicated by the detection of free complex IV. Overall, the respiratory supercomplex profile for Δ*aac2*Δ*crd1* extracts resembled that observed for Δ*crd1* extracts with one notable difference: the $III_2IV$ to $III_2IV_2$ ratio was even further skewed in the $III_2IV$ direction when AAC2 and CL were both missing. Importantly, the normal assembly/stability of complex V demonstrated that the formation of protein complexes in the mitochondrial IM was not generally impaired in any of these strains. Collectively, both AAC2 and CL are required for the normal assembly and/or stability of the respiratory supercomplexes. Moreover, the increased mobility of the supercomplexes in the Δ*crd1* extracts likely reflects the cumulative absence of bound CL, associated AAC2, and perhaps additional unidentified subunits that require CL to interact with the respiratory supercomplexes. Lastly, given the cumulative impact on the respiratory supercomplexes by the combined absence of both AAC2 and CL, AAC2 and CL are likely to have at least partially distinct roles with respect to respiratory supercomplex composition and/or stability.

To determine if any of the observed structural alterations in the respiratory supercomplexes are associated with deficits in function, we analyzed the respiratory activity in the purified mitochondria (Fig. 6). State III respiration rate is a measure of ADP-stimulated oxygen consumption and is probably the most commonly used parameter to evaluate mitochondrial respiratory function. After all ADP is used for ATP synthesis, respiration slows down to state IV, due to limitation of electron transfer and proton pumping by the high proton gradient. The ratio of state III to state IV respiration (RCR, or respiratory control ratio) is an indication of mitochondrial energetic coupling and membrane stability. Moreover, it is possible to assess the efficiency of ATP synthesis per oxygen atom reduced (ADP:O ratio) by measuring the amount of oxygen consumed after the addition of a known amount of ADP. Using substrates that enter the ETC at different points, specific defects of the respiratory chain can be localized. Therefore, we used NADH (external NADH dehydrogenase substrate), succinate (complex II substrate), and ascorbate + TMPD (complex IV substrate) to analyze the respiratory function of wt, Δ*crd1*, Δ*aac2*, Δ*taz1*, *and* Δ*aac2*Δ*crd1* mitochondria.

In the absence of AAC2, even when either AAC1 or AAC3 could theoretically replace AAC2, the RCR values were "1" with all three different substrates, reflecting a lack of ADP/ATP exchange across the IM. Therefore, with respect to a possible influence of AAC2 on ETC function, the most relevant parameters are the basal state IV and maximum uncoupled respiration rates (when the proton gradient is collapsed by CCCP, the activities of the ATP synthase and the respiratory supercomplexes are uncoupled, resulting in increased substrate utilization and concomitant oxygen consumption). Previous studies have suggested that in the absence of AAC2 some of the cytochromes associated with complexes III and IV may be less abundant (Muller et al., 1996). Thus, in theory, any reduction in maximum uncoupled respiration rates of Δ*aac2* mitochondria could

reflect a reduced amount or activity of functional complexes III or IV. However, that there were no gross alterations in the respiratory supercomplexes in the absence of AAC2 would seem to argue against this possibility. Indeed, we observed reduced complex IV activity (80 ± 5.4%) with ascorbate + TMPD, and even further impaired ETC activity with NADH (72 ± 7.9%) and succinate (78 ± 5.3%). This result indicates that AAC2 is required for maximal ETC activity even in the uncoupled state, where ADP/ATP translocase activity is bypassed. Notably, the reduced complex IV activity in the absence of AAC2, despite normal levels of complex IV proteins, points to a role for AAC2 in supporting complex IV function.

In contrast, Δ*crd1* mitochondrial respiratory function is severely affected. In the absence of CL, with all three respiratory substrates, state III (62–72%; Fig. 6 B and Table S4, available at http://www.jcb.org/cgi/content/full/jcb.200801152/DC1) and ATP synthesis (46 ± 0.003%; Fig. 6 F and Table S4) rates were significantly lower than in wt mitochondria. The calculated RCR for the Δ*crd1* mitochondria was also significantly reduced (76–83%; Fig. 6 A and Table S4), as reported previously (Koshkin and Greenberg, 2000). Moreover, the ADP:O ratio (Fig. 6 E) of Δ*crd1* mitochondria was 65 ± 4.8% of wt, indicating that CL is necessary for efficient harvesting of the proton gradient toward ATP synthesis. Strikingly, the extent of reduction in ATP synthesis (46 ± 0.003%) with NADH could be calculated by multiplying the additive effects of state III oxygen consumption (72 ± 4%) and the efficiency of ATP synthesis per oxygen (ADP:O, 65 ± 4.8%). Therefore, the reduced respiratory function of Δ*crd1* mitochondria is a combination of the reduced capacity of the ETC and the reduced efficiency of ATP synthesis.

The sensitivity of state III respiration to inhibition by atractyloside was reduced in Δ*crd1* mitochondria (Fig. 6 D and Table S4). Given that atractyloside completely inhibited ATP synthesis in both wt and Δ*crd1* mitochondria (unpublished data), this difference is not due to an incomplete inhibition of AAC2, but rather points to its decreased control over state III respiration in Δ*crd1* mitochondria, possibly caused by impaired complex IV activity (Koshkin and Greenberg, 2000). Indeed, in the presence of ascorbate + TMPD and the uncoupler, CCCP, complex IV activity in Δ*crd1* mitochondria was reduced by 46 ± 2.3% (Table S4). Additionally, this reduction in complex IV activity resulted in lower uncoupled rates with NADH and succinate (55–65%; Fig. 6 C and Table S4).

Significantly, the combined absence of AAC2 with CL (Δ*aac2*Δ*crd1*) had an even more drastic effect on all the respiratory parameters than of CL or AAC2 alone (Fig. 6 and Table S4). An even further impaired complex IV activity of Δ*aac2*Δ*crd1* compared with Δ*crd1* mitochondria also suggests that cooperation between CL and AAC2 is required for maximum complex IV incorporation into supercomplexes and activity. Moreover, it suggests that the lower complex IV activity of Δ*aac2* mitochondria is not due to any alteration of CL organization, levels, etc., but it is more likely due to the absence of a direct interaction between AAC2 and the respiratory supercomplex. In sum, these data indicate that AAC2 and CL have distinct and yet partially overlapping roles with respect to the structural arrangement and optimal functioning of the respiratory supercomplexes.

The respiratory parameters of Δ*taz1* mitochondria were only moderately affected compared with Δ*crd1* mitochondria (Fig. 6 and Table S4). Complex IV activity was reduced to 72 ± 2% that of wt, and state III respiration was affected only in the presence of succinate but not NADH (77 ± 4% and 108 ± 7%, respectively). Moreover, both the decrease in uncoupled respiration rate and the calculated RCR was more prominent in the presence of succinate than NADH. Substrate-specific differences in respiratory function of Δ*taz1* mitochondria have been reported previously (Ma et al., 2004). Overall, the absence of Taz1p causes moderate changes in respiratory supercomplex function and no discernable defects in assembly.

## Discussion

Virtually nothing is known about the interactome of the mitochondrial ADP/ATP carrier. Therefore, a more complete definition of proteins that interact with AAC will provide insight into normal physiological processes as well as certain pathological conditions linked to AAC function/dysfunction. To this end, we have focused our attention on yeast AAC2 and added the extra wrinkle of examining the influence of CL on the defined AAC2 interactome. Our rationale for focusing on yeast AAC2 is that (1) it has been subjected to extensive mutagenesis and structure–function studies, (2) it is widely regarded as a model for the mitochondrial carrier family in general, and (3) it has been demonstrated as a relevant model to study mutations found in the ANT1 protein in human patients suffering from PEO (Nelson et al., 1993; Muller et al., 1996; Fontanesi et al., 2004; Palmieri et al., 2005). Moreover, a large body of work collectively indicates that CL is uniquely important for AAC structure and function (Hoffmann et al., 1994; Beyer and Nuscher, 1996; Jiang et al., 2000). Additionally, CL peroxidation has been linked to cytochrome *c* (cyt *c*) release in the early stages of apoptosis (Ott et al., 2007); CL oxidation, reduced CL levels, and/or altered molecular composition linked to the mitochondrial dysfunction associated with aging, ischemia and reperfusion, and Barth syndrome (Chicco and Sparagna, 2007); and deficits in CL synthesis and increased CL catabolism connected to diabetic cardiomyopathy (Han et al., 2005). Therefore, the pathological insults affiliated with any of these conditions could in theory involve alterations in the AAC interactome caused by the altered mitochondrial lipid environment observed in these disease states.

We developed a new dual affinity tag and system, termed CNAP. Attachment of the CNAP tag to the N terminus of AAC2 followed by preparative scale consecutive nondenaturing affinity purification revealed that AAC2 interacts with the respiratory supercomplexes, other mitochondrial carriers, and potentially other proteins and complexes. Moreover, the CNAP tag and strategy allowed us to assign these interactions to AAC2-containing complexes of defined size. Specifically, AAC2 associates with respiratory supercomplexes of >669 kD and other mitochondrial carriers in complexes that range in size from ~400 kD to 160 kD. The importance of CL in the AAC2 interactome is obvious both with respect to the profile/intensity of co-affinity purified proteins and, as best indicated by the association with the respiratory supercomplexes, the size of the AAC2-interacting

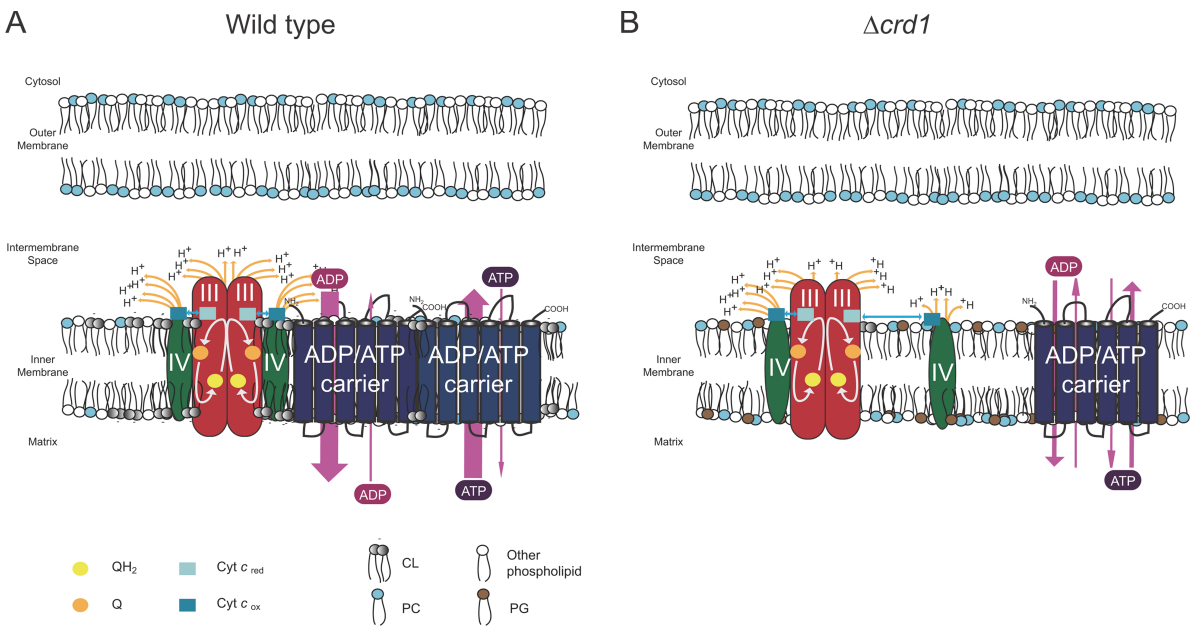


Figure 7. **Model for how CL increases the efficiency of oxidative phosphorylation.** (A) CL, the "green" phospholipid, not only facilitates cyt *c* (blue squares) transport between complexes III (red ovals) and IV (dark green ovals) by stabilizing the $III_2IV_2$+AAC2 supercomplex, but additionally stimulates AAC (six membrane domains represented by blue cylinders) activity by placing it in an electrochemical bath provided by the proton-coupled electron transport activity of complexes III and IV. (B) In the absence of CL, the net distance traveled by cyt *c* between complexes III and IV is increased and the potential benefits on AAC2 function by associating with the respiratory supercomplexes is lost, resulting in a reduced efficiency of OXPHOS. Not drawn to scale.

complexes. Both parameters reflect functional consequences of the absence of CL with respect to the AAC2 interactome, as clearly demonstrated for the respiratory supercomplexes.

### Cardiolipin, the "green" phospholipid

The main argument used to rationalize the presence of the respiratory supercomplexes is that the physical association between complexes III and IV increases the efficiency of substrate channeling, specifically of cyt *c* between these complexes. As schematized in Fig. 7 A, reduced ubiquinol ($QH_2$) is converted to quinone (Q) through the reduction of cyt *c* (cyt $c_{red}$) which then must shuttle to complex IV. Using oxygen as the terminal electron acceptor, complex IV oxidizes cyt $c_{red}$, generating oxidized cyt *c* (cyt $c_{ox}$). Cyt $c_{ox}$ can then reassociate with complex III and participate in another redox cycle. In the absence of CL (Fig. 7 B), the association of complex IV with the respiratory supercomplexes is destabilized. This is reflected by the increased abundance of the $III_2IV$ form of the supercomplex, which potentially decreases the overall efficiency of cyt *c* shuttling due to the increased distance between the dissociated complex IV and the $III_2IV$ supercomplex.

An end result of complex III and IV activity is the pumping of protons across the IM. Thus, the physical association of complex III and IV not only results in the enhanced efficiency of electron flow between these complexes, but it also effectively combines and increases their respective proton-transporting capacities. As such, the local microenvironment might be anticipated to exhibit a relatively high electrochemical gradient. Interestingly, both the directionality and activity of ADP/ATP carriers are known to be influenced by the electrochemical gradient. Specifically, in the presence of a positive membrane potential, transport of ATP out of the matrix is significantly favored over transport of ATP into the matrix (Kramer and Klingenberg, 1980). Given that transport of ATP out of the matrix requires the coincident transport of ADP into the matrix, the membrane potential essentially establishes the directionality of AAC transport. Transport of ATP out of and ADP into the matrix is known to be energetically costly due to the partial collapse of the membrane potential upon the release of ATP and its extra negative charge. We speculate that the association of AAC2 with the respiratory supercomplexes places it in an area with a uniquely high local electrochemical gradient. This high local electrochemical gradient enforces the directionality and activity of adenine nucleotide transport (reflected by thickness of pink arrows in Fig. 7). Essentially, the juxtaposition of AAC2 with the only respiratory complexes that mediate electron-coupled proton transport in yeast increases the efficiency of AAC2 function, which is required for OXPHOS. In the absence of CL (Fig. 7 B), the association of AAC2 with the respiratory supercomplexes is diminished or abolished, resulting in a reduced coupling of proton transport to ATP production.

However, the benefits of this association between AAC2 and the respiratory supercomplexes is by no means one-sided, as we demonstrated that in the absence of AAC2, ETC and specifically complex IV activity is significantly decreased (Fig. 6, Table S4), in agreement with previous papers (Heidkamper et al., 1996; Muller et al., 1996; Fontanesi et al., 2004). Our observations revealed limited structural changes in respiratory supercomplexes and 20% reduction in complex IV activity in the absence of AAC2. It is difficult to correlate the extent of

structural change to activity, as complex IV is still active when it is not incorporated into respiratory supercomplexes. Thus, how AAC2 contributes to complex IV and ETC activity is presently not clear. Although CL is essential for both AAC2 and complex IV activity, AAC2 has a distinct role in respiratory supercomplex assembly and function that cannot be replaced by CL or any other endogenous protein.

As discussed above, CL may contribute to the efficiency of OXPHOS both by decreasing the distance through which cyt *c* must travel between complexes III and IV as well as placing AAC2 in an environment that promotes its optimal activity. Perhaps the contribution of CL to the efficiency of OXPHOS is best revealed by the significant drop in the ADP:O ratio in the absence of CL. As such, we suggest that the drop in ADP:O ratio observed in the Δ*crd1* mitochondria relative to wt mitochondria provides a rough estimate of the energy savings provided by CL. Although lower respiratory capacity and efficiency for Δ*crd1* mitochondria has been reported (Koshkin and Greenberg, 2000), the molecular mechanism(s) responsible for these observations were not provided. With the AAC2 interactome defined herein, we for the first time, provide a model where the physical interaction of AAC2 with respiratory supercomplexes is at least partially responsible for the more efficient and faster ATP production in the presence versus the absence of CL. Thus, through facilitating respiratory supercomplex assembly and recruiting AAC2, we conclude that under optimal conditions, CL increases the efficiency of OXPHOS by at least 35%. In today's world of green technologies, CL's impact on the efficiency of OXPHOS would be enviable and as such, CL should be regarded as the mitochondrion's "green" phospholipid.

## Materials and methods

### Molecular biology

AAC2, including ~350 bps 5′ UTR and ~70 bps 3′ UTR, was amplified by PCR using genomic DNA isolated from the GA74-6A yeast strain as template and subcloned into the centromeric vector, pRS315. To place the CNAP tag (amino acid sequence MEDQVDPRLIDGK–GGAGG–**HHHHHHHHHH**; PC epitope tag underlined and $His_{10}$ tag in bold) onto the N terminus of AAC2 but still under control of the AAC2 promoter, overlap extension was performed (Ho et al., 1989). The sequence of every construct was verified by DNA sequencing. The sequences of all primers are available upon request.

### Yeast strains

All strains were derived from the WT parental *S. cerevisiae* yeast strains GA74-1A (*MAT a, his3 -11,15, leu2, ura3, trp1, ade8, rho*$^+$*, mit*$^+$) or GA74-6A (*MAT* α*, his3 -11,15, leu2, ura3, trp1, ade8, rho*$^+$*, mit*$^+$). The Δ*taz1* (*MAT a, leu2, ura3, trp1, ade8, Δtaz1::HISMX6*) has been described previously (Claypool et al., 2006). To generate the Δ*aac2* (*MAT a, leu2, ura3, trp1, ade8, Δaac2::HISMX6*), Δ*crd1* (*MAT a, his3 -11,15, leu2, ura3, ade8, Δcrd1::TRP*), Δ*aac2*Δ*crd1* (*MAT a, leu2, ura3, ade8, Δaac2::HISMX6, Δcrd1::TRP*), Δ*mir1* (*MAT* α*, leu2, ura3, ade8, his3 -11,15, Δmir1::TRP*), Δ*aac2*Δ*mir1* (*MAT a, leu2, ura3, ade8, Δaac2::HISMX6, Δmir1::TRP*), Δ*ggc1* (*MAT* α*, leu2, ura3, ade8, his3 -11,15, Δggc1::TRP*) and Δ*aac2*Δ*ggc1* (*MAT a, leu2, ura3, ade8, Δaac2::HISMX6, Δggc1::TRP*) strains, the entire open reading frame of each gene was replaced using the PCR-mediated one-step gene replacement strategy (Wach et al., 1994).

### 2D blue native/SDS-PAGE

1D BN-PAGE was performed as described previously (Claypool et al., 2006). Before resolution in the second dimension by SDS-PAGE, the BN-PAGE gel was soaked in 1% (wt/vol) SDS, 1% (vol/vol) β-mercaptoethanol for 30 min at 50°C, and individual lanes, isolated with a razor blade, embedded in a 4% stacking gel.

### Antibodies

Most of the antibodies used in this work were generated in the Schatz laboratory or our laboratory and have been described previously. Other antibodies used were: mouse anti-Sec62p (a gift of Dr. David Meyers, University of California, Los Angeles, Los Angeles, CA), mouse anti-RIP1 (a gift of Dr. Bernard Trumpower, Dartmouth Medical School, Hanover, NH), mouse anti-yAAC2 (clone 6H8; Panneels et al., 2003), and horseradish peroxidase–conjugated secondary antibodies (Thermo Fisher Scientific).

### CNAP

Detergent solubilization of mitochondria (5 mg/ml) was performed for 30 min on ice with 20 mM Hepes-KOH, pH 7.4, 20 mM imidazole, 10% glycerol, 100 mM NaCl, and 1 mM $CaCl_2$, supplemented with 1.5% (wt/vol) digitonin (Biosynth International, Inc.) and protease inhibitors (1 mM PMSF, 10 µM leupeptin, 2 µM pepstatin A, and 10 µM chymostatin). Insoluble material was removed at 20,000 *g* for 30 min at 4°C and extracts transferred to 15-ml falcon tubes containing 8 ml lysis buffer base with added protease inhibitors and 0.8 ml NiNTA resin (QIAGEN). After 1 h rotating at 4°C, the contents were poured into a column, the resin allowed to settle briefly, and the flow-thru collected. After two washes with 8 ml lysis buffer base containing 0.1% (wt/vol) digitonin, bound material was directly eluted into separate columns containing 1 ml equilibrated anti-PC resin (Roche; equilibration buffer 20 mM Hepes-KOH, pH 7.4, 100 mM NaCl, and 1 mM $CaCl_2$) with 8 ml $Ni^{2+}$ elution buffer (20 mM Hepes-KOH, pH 7.4, 300 mM imidazole, 10% glycerol, 100 mM NaCl, 1 mM $CaCl_2$, and 0.1% digitonin). After 1 h rotating at 4°C, the flow-thru was collected and the columns washed twice with 10 ml anti-PC wash buffer (anti-PC equilibration buffer with 0.1% digitonin). To elute bound material, the columns were capped and 1 ml of EDTA elution solution (20 mM Hepes-KOH, pH 7.4, 100 mM NaCl, 5 mM EDTA, and 0.1% digitonin) was added to the anti-PC resin. Four elutions were performed. The first elution consisted of 15 min at 4°C and then 15 min at room temperature; the remaining three elutions were at room temperature. Eluates were directly pooled in Amicon filtration devices, 10,000 MWCO kept on ice and the pooled eluates concentrated following the provided guidelines (Millipore). For the ATP2CNAP used as an additional negative control (Fig. S1), 0.05% (wt/vol) SDS was included in the EDTA elution solution. Concentrated CNAPed product derived from 4 and 10 mg starting material was analyzed in the preparative 1D and 2D BN/SDS-PAGE analyses, respectively, and proteins revealed with the SYPRO Ruby stain and protocol (Invitrogen).

### Liquid chromatography–mass spectrometry

Gels were imaged and analyzed with PDQuest (Bio-Rad Laboratories) software. Protein bands of interest were excited by a spot-excision robot (Proteome Works; Bio-Rad Laboratories) and deposited into 96-well plates. Gel bands were digested with sequencing-grade trypsin (Promega), and the resulting tryptic peptides were extracted using standard protocol (Shevchenko et al., 1996). LC–MS/MS of peptide mixtures was performed on a QSTAR Pulsar XL (QqTOF) mass spectrometer (Applied Biosystems) equipped with nanoelectrospray interface (Protana) and LC Packings nano-LC system. The nano-LC was equipped with homemade precolumn (150 µm × 5 mm) and analytical column (75 µm × 150 mm) packed with Jupiter Proteo C12 resin (particle size 4 µm; Phenomenex). The dried peptides were resuspended in 1% formic acid (FA) solution. 6 µl of sample solution was loaded to the precolumn for each LC–MS/MS run. The precolumn was washed with the loading solvent (0.1% FA) for 4 min before the sample was injected onto the LC column. The eluants used for the LC were 0.1% FA (solvent A) and 95% ACN containing 0.1% FA (solvent B). The flow rate was 200 nL/min, and the following gradient was used: 3% B to 6% B in 6 s, 6% B to 24% B in 18 min, 24% B to 36% B in 6 min, 36% B to 80% B in 2 min, and maintained at 80% B for 7.9 min. The column was finally equilibrated with 3% B for 15 min before the next run. Electrospray ionization was performed using a 30-µm (i.d.) nano-bore stainless steel online emitter (Proxeon) and a voltage set at 1900 V. Protein identification was accomplished using the Mascot database search engine (Matrix Science). All searches were performed against the Swiss-Prot protein sequence database, allowing for phosphorylated, Ser, Thr and Tyr, oxidized Met, carbamidomethylated Cys, and N-terminal pyro-Gly, and using a mass tolerance of 0.3 D.

### Immunoprecipitation

Antisera raised against the complex IV holoenzyme or normal rabbit serum as a negative control was conjugated to protein A–sepharose using the Seize X Protein A Immunoprecipitation kit and protocol (Thermo Fisher Scientific). Alternatively, the monoclonal antibody reactive to the N terminus of yeast AAC2, 6H8, or normal mouse serum as negative control was

conjugated to protein G–sepharose as just described. After solubilization and clarification as described above, 0.5 mg mitochondrial extract derived from the indicated strains was added to microfuge tubes containing 70 µl normal rabbit serum–conjugated beads and 1.1 ml lysis buffer base supplemented with protease inhibitors and incubated for 1 h at 4°C with rotation. For the anti-AAC2 IP, 1 mg mitochondrial extract derived from the indicated strains was added to microfuge tubes containing 70 µl normal mouse serum–conjugated beads and 0.9 ml lysis buffer base supplemented with protease inhibitors and incubated for 1 h at 4°C with rotation. After centrifugation at 2,000 rpm at 4°C, the pre-cleared lysates were transferred to tubes containing 70 µl anti-complex IV or anti-AAC2–conjugated beads and incubated for 4 h at 4°C with rotation. After low speed centrifugation as before, the nonbinding flow-thru was collected for analysis and the bound material (both the preclear and IP beads) was washed three times with 1 ml lysis buffer base containing 0.1% digitonin, 10 min rotating at 4°C/wash. To elute bound material, three sequential elutions were performed using 0.1M glycine, pH 2.8, supplemented with 0.1% digitonin, and the pooled eluates were first neutralized with 50 µl 1M Tris-Cl, pH 8.0, and then concentrated using Microcon YM-10 filter devices and guidelines (Millipore). This elution protocol allowed the reuse of the conjugated columns at least three times.

### Mitochondrial respiration and ATP production measurements

A mitochondrial aliquot (25 mg/ml) was thawed on ice before each experiment and used within 2 h. Oxygen consumption of mitochondria was measured using a Clark-type oxygen electrode in a magnetically stirred, thermostatically controlled 1.5-ml chamber at 25°C (Oxytherm; Hansatech). 100 (for NADH and ascorbate + TMPD) or 200 µg (for succinate) mitochondria were resuspended in 0.25 M sucrose, 0.25 mg/ml BSA, 20 mM KCl, 20 mM Tris-Cl, 0.5 mM EDTA, 4 mM $KH_2PO_4$, and 3 mM $MgCl_2$, pH 7.2, as modified from Jiang et al., (2000). After addition of 5 mM succinate, or 2 mM NADH, or 1 mM ascorbate + 0.3 mM TMPD, state II rate was monitored for approximately 1 min. State III respiration was initiated by addition of 50 µM ADP. After state IV rate was measured, 100 µM ADP was added, which was followed by inhibition of AAC by 40 µM atractyloside. 10 µM oligomycin was used to see if atractyloside inhibition was complete. Finally, 10 µM CCCP was added to induce uncoupled respiration, and the rate was followed until oxygen level reached zero.

Mitochondrial ATP production rate was measured using the same conditions as described for NADH respiration, except that 200 µg mitochondria was used and 10 µM $Ap_5A$ was added to eliminate ATP production by adenylate kinase. Also, 2 mM ADP was added to start ATP synthesis. Every 30 s after ADP addition, 10-µl aliquots were removed and incubated with 10 µl ice-cold 4% PCA for 5 min. 1.5 ml of 0.5M Tris-Acetate was added to neutralize the solution and the extracts were kept at 4°C overnight. ATP content of each extract was measured using the Enliten kit and protocol (Promega). Luminescence was measured using a Lumat LB 9507 (EG & Berthold). Control experiments using 40 µM atractyloside were performed to demonstrate AAC dependency of ATP production by complex V, and ATP production was essentially zero in the presence of atractyloside. Statistical comparisons were performed using SigmaStat 3 software (Systat Software, Inc.).

### Miscellaneous

Subcellular fractionation, isolation of mitochondria, and immunoblotting was as described previously (Claypool et al., 2006). The performed experiments used mitochondria harvested from yeast grown at 30°C to $OD_{600}$ ~3 in: Fig. 1, A and D (top 2 panels), and Fig. 4 E, rich lactate medium (1% yeast extract, 2% tryptone, 0.05% dextrose, and 2% lactic acid, 3.4 mM $CaCl_2$ $2H_2O$, 8.5 mM NaCl, 2.95 mM $MgCl_2$ $6H_2O$, 7.35 mM $KH_2PO_4$, and 18.7 mM $NH_4Cl$); Fig. 1, B and D (bottom three panels), Fig. 2, and Fig. 3, synthetic lactate −Leu (0.17% yeast nitrogen base minus amino acids and ammonium sulfate, 0.5% ammonium sulfate, 0.2% Dropout Mix Synthetic −Leu, 0.05% dextrose, and 2% lactic acid, 3.4 mM $CaCl_2$ $2H_2O$, 8.5 mM NaCl, 2.95 mM $MgCl_2$ $6H_2O$, 7.35 mM $KH_2PO_4$, and 18.7 mM $NH_4Cl$); and Fig. 4, A–D, Fig. 5, and Fig. 6, YP-dextrose. Phospholipid labeling and extraction and data collection was as described previously (Claypool et al., 2006), except that the extracted phospholipids were resolved only 1X on the TLC plates. Statistical comparisons were performed using SigmaStat 3 software.

### Online supplemental material

Fig. S1 presents an additional negative control for the CNAP tag. Tables S1–S3 present the LC–MS/MS data generated for Figs. 2 and 3. Table S4 summarizes the respiratory studies. Online supplemental material available at http://www.jcb.org/cgi/content/full/jcb.200801152/DC1.

We would like to thank Dr. Jeff Schatz for antibodies, Drs. Bernard Trumpower and Irmgard Sinning for the anti-RIP1 and anti-AAC2 monoclonal antibodies, respectively, and Dr. Deepa Dabir and Samuel Hasson of the Koehler laboratory for technical guidance.

This work was supported by the American Heart Association 0640076N, Muscular Dystrophy Association (4033), and National Institutes of Health grants R01GM61721 (CMK), R01GM07398 (CMK), R01RR20004 (JAL), and K99HL089185-01 (S.M. Claypool). The UCLA Mass Spectrometry and Proteomics Technology Center was established with a grant from the W.M. Keck Foundation. C.M. Koehler is an Established Investigator of the American Heart Association.

Submitted: 24 January 2008
Accepted: 11 August 2008

## References

Beyer, K., and B. Nuscher. 1996. Specific cardiolipin binding interferes with labeling of sulfhydryl residues in the adenosine diphosphate/adenosine triphosphate carrier protein from beef heart mitochondria. *Biochemistry.* 35:15784–15790.

Boumans, H., L.A. Grivell, and J.A. Berden. 1998. The respiratory chain in yeast behaves as a single functional unit. *J. Biol. Chem.* 273:4872–4877.

Brandner, K., D.U. Mick, A.E. Frazier, R.D. Taylor, C. Meisinger, and P. Rehling. 2005. Taz1, an outer mitochondrial membrane protein, affects stability and assembly of inner membrane protein complexes: implications for Barth Syndrome. *Mol. Biol. Cell.* 16:5202–5214.

Chicco, A.J., and G.C. Sparagna. 2007. Role of cardiolipin alterations in mitochondrial dysfunction and disease. *Am. J. Physiol. Cell Physiol.* 292:C33–C44.

Claypool, S.M., J.M. McCaffery, and C.M. Koehler. 2006. Mitochondrial mislocalization and altered assembly of a cluster of Barth syndrome mutant tafazzins. *J. Cell Biol.* 174:379–390.

Cruciat, C.M., S. Brunner, F. Baumann, W. Neupert, and R.A. Stuart. 2000. The cytochrome bc1 and cytochrome c oxidase complexes associate to form a single supracomplex in yeast mitochondria. *J. Biol. Chem.* 275:18093–18098.

Fontanesi, F., L. Palmieri, P. Scarcia, T. Lodi, C. Donnini, A. Limongelli, V. Tiranti, M. Zeviani, I. Ferrero, and A.M. Viola. 2004. Mutations in AAC2, equivalent to human adPEO-associated ANT1 mutations, lead to defective oxidative phosphorylation in *Saccharomyces cerevisiae* and affect mitochondrial DNA stability. *Hum. Mol. Genet.* 13:923–934.

Hackenberg, H., and M. Klingenberg. 1980. Molecular weight and hydrodynamic parameters of the adenosine 5′-diphosphate–adenosine 5′-triphosphate carrier in Triton X-100. *Biochemistry.* 19:548–555.

Han, X., J. Yang, H. Cheng, K. Yang, D.R. Abendschein, and R.W. Gross. 2005. Shotgun lipidomics identifies cardiolipin depletion in diabetic myocardium linking altered substrate utilization with mitochondrial dysfunction. *Biochemistry.* 44:16684–16694.

Heidkamper, D., V. Muller, D.R. Nelson, and M. Klingenberg. 1996. Probing the role of positive residues in the ADP/ATP carrier from yeast. The effect of six arginine mutations on transport and the four ATP versus ADP exchange modes. *Biochemistry.* 35:16144–16152.

Heinemeyer, J., H.P. Braun, E.J. Boekema, and R. Kouril. 2007. A structural model of the cytochrome *C* reductase/oxidase supercomplex from yeast mitochondria. *J. Biol. Chem.* 282:12240–12248.

Ho, S.N., H.D. Hunt, R.M. Horton, J.K. Pullen, and L.R. Pease. 1989. Site-directed mutagenesis by overlap extension using the polymerase chain reaction. *Gene.* 77:51–59.

Hoffmann, B., A. Stockl, M. Schlame, K. Beyer, and M. Klingenberg. 1994. The reconstituted ADP/ATP carrier activity has an absolute requirement for cardiolipin as shown in cysteine mutants. *J. Biol. Chem.* 269:1940–1944.

Jiang, F., M.T. Ryan, M. Schlame, M. Zhao, Z. Gu, M. Klingenberg, N. Pfanner, and M.L. Greenberg. 2000. Absence of cardiolipin in the crd1 null mutant results in decreased mitochondrial membrane potential and reduced mitochondrial function. *J. Biol. Chem.* 275:22387–22394.

Koehler, C.M., M.P. Murphy, N.A. Bally, D. Leuenberger, W. Oppliger, L. Dolfini, T. Junne, G. Schatz, and E. Or. 2000. Tim18p, a new subunit of the TIM22 complex that mediates insertion of imported proteins into the yeast mitochondrial inner membrane. *Mol. Cell. Biol.* 20:1187–1193.

Koshkin, V., and M.L. Greenberg. 2000. Oxidative phosphorylation in cardiolipin-lacking yeast mitochondria. *Biochem. J.* 347:687–691.

Kramer, R., and M. Klingenberg. 1980. Modulation of the reconstituted adenine nucleotide exchange by membrane potential. *Biochemistry.* 19:556–560.

Ma, L., F.M. Vaz, Z. Gu, R.J. Wanders, and M.L. Greenberg. 2004. The human TAZ gene complements mitochondrial dysfunction in the yeast taz1Delta mutant. Implications for Barth syndrome. *J. Biol. Chem.* 279:44394–44399.

Muller, V., G. Basset, D.R. Nelson, and M. Klingenberg. 1996. Probing the role of positive residues in the ADP/ATP carrier from yeast. The effect of six arginine mutations of oxidative phosphorylation and AAC expression. *Biochemistry.* 35:16132–16143.

Nelson, D.R., J.E. Lawson, M. Klingenberg, and M.G. Douglas. 1993. Site-directed mutagenesis of the yeast mitochondrial ADP/ATP translocator. Six arginines and one lysine are essential. *J. Mol. Biol.* 230:1159–1170.

Ott, M., B. Zhivotovsky, and S. Orrenius. 2007. Role of cardiolipin in cytochrome *c* release from mitochondria. *Cell Death Differ.* 14:1243–1247.

Palmieri, L., S. Alberio, I. Pisano, T. Lodi, M. Meznaric-Petrusa, J. Zidar, A. Santoro, P. Scarcia, F. Fontanesi, E. Lamantea, et al. 2005. Complete loss-of-function of the heart/muscle-specific adenine nucleotide translocator is associated with mitochondrial myopathy and cardiomyopathy. *Hum. Mol. Genet.* 14:3079–3088.

Panneels, V., U. Schussler, S. Costagliola, and I. Sinning. 2003. Choline head groups stabilize the matrix loop regions of the ATP/ADP carrier ScAAC2. *Biochem. Biophys. Res. Commun.* 300:65–74.

Pfeiffer, K., V. Gohil, R.A. Stuart, C. Hunte, U. Brandt, M.L. Greenberg, and H. Schagger. 2003. Cardiolipin stabilizes respiratory chain supercomplexes. *J. Biol. Chem.* 278:52873–52880.

Schagger, H., and K. Pfeiffer. 2000. Supercomplexes in the respiratory chains of yeast and mammalian mitochondria. *EMBO J.* 19:1777–1783.

Schlame, M. 2008. Cardiolipin synthesis for the assembly of bacterial and mitochondrial membranes. *J. Lipid Res.* 49:1607–1620.

Schlame, M., and D. Haldar. 1993. Cardiolipin is synthesized on the matrix side of the inner membrane in rat liver mitochondria. *J. Biol. Chem.* 268:74–79.

Schlame, M., D. Rua, and M.L. Greenberg. 2000. The biosynthesis and functional role of cardiolipin. *Prog. Lipid Res.* 39:257–288.

Sedlak, E., and N.C. Robinson. 1999. Phospholipase A(2) digestion of cardiolipin bound to bovine cytochrome c oxidase alters both activity and quaternary structure. *Biochemistry.* 38:14966–14972.

Sharer, J.D. 2005. The adenine nucleotide translocase type 1 (ANT1): a new factor in mitochondrial disease. *IUBMB Life.* 57:607–614.

Shevchenko, A., M. Wilm, O. Vorm, and M. Mann. 1996. Mass spectrometric sequencing of proteins silver-stained polyacrylamide gels. *Anal. Chem.* 68:850–858.

Vyssokikh, M.Y., and D. Brdiczka. 2003. The function of complexes between the outer mitochondrial membrane pore (VDAC) and the adenine nucleotide translocase in regulation of energy metabolism and apoptosis. *Acta Biochim. Pol.* 50:389–404.

Wach, A., A. Brachat, R. Pohlmann, and P. Philippsen. 1994. New heterologous modules for classical or PCR-based gene disruptions in *Saccharomyces cerevisiae*. *Yeast.* 10:1793–1808.

Xu, Y., A. Malhotra, M. Ren, and M. Schlame. 2006. The enzymatic function of tafazzin. *J. Biol. Chem.* 281:39217–39224.

Zhang, M., E. Mileykovskaya, and W. Dowhan. 2002. Gluing the respiratory chain together. Cardiolipin is required for supercomplex formation in the inner mitochondrial membrane. *J. Biol. Chem.* 277:43553–43556.

Zhang, M., X. Su, E. Mileykovskaya, A.A. Amoscato, and W. Dowhan. 2003. Cardiolipin is not required to maintain mitochondrial DNA stability or cell viability for *Saccharomyces cerevisiae* grown at elevated temperatures. *J. Biol. Chem.* 278:35204–35210.

Zhang, M., E. Mileykovskaya, and W. Dowhan. 2005. Cardiolipin is essential for organization of complexes III and IV into a supercomplex in intact yeast mitochondria. *J. Biol. Chem.* 280:29403–29408.